

**UCSF**

**UC San Francisco Electronic Theses and Dissertations**

**Title**

Comparison of Computational Fluid Dynamics (CFD) and Magnetic Resonance Velocimetry (MRV) in a Flow Model

**Permalink**

<https://escholarship.org/uc/item/5wz270sb>

**Author**

Zhang, Xinheng

**Publication Date**

2016

Peer reviewed|Thesis/dissertation

Comparison of Computational Fluid Dynamics (CFD) and Magnetic  
Resonance Velocimetry (MRV) in a Flow Model

by

Xinheng Zhang

THESIS

Submitted in partial satisfaction of the requirements for the degree of

MASTER OF SCIENCE

in

Biomedical Imaging

in the

GRADUATE DIVISION

of the

UNIVERSITY OF CALIFORNIA, SAN FRANCISCO



**Copyright 2016**

**By**

**Xinheng Zhang**

## **Dedication and acknowledgements**

First and foremost, this publication and all related work is dedicated to my thesis advisor David Saloner. I thank him for guiding me in every aspect of the project and helping me to maintain reasonable expectations of research but persistent faith in my goal as well.

Thanks to Evan Kao, Henrik Haraldsson, Sarah Kefayati, Sravani Kondapavulur and Eric Chow for providing me with generous help ranging from 3D printing, MR scanning, image data processing to CFD simulation. Without their help, there is no way I could have completed this thesis paper.

Additionally, I'm grateful to all the MSBI classmates for studying with, accompany with, and supporting me during this year's program. It's been an unforgettable experience of my life. I wish them all the best in the future.

Lastly, I'm grateful to my thesis committee members who reviewed and gave advice on my work.

## Abstract

**Introduction:** Information from MR blood flow quantification can be used to evaluate patient health, inform surgical decisions and provide boundary conditions for numerical simulations. Thus, it is important to determine the accuracy and precision of the flow measurement and its contributing factors. In this study, we investigated the reproducibility of the measurement by comparing flow results from 2D MRV, 4D MRV and CFD. Also, we investigated the sensitivity of the measurements at different positions in the scanner, since these could be affected by gradient field imperfections.

**Methods:** A phantom which was an exact replica of a patient intracranial aneurysm was set up with a flow system where flow was driven by a gravity-fed pressure head to provide constant flow. A contrast-enhanced MRA image was obtained at 0.5 mm isotropic resolution to determine the geometry. 4D MRV within the phantom was measured under 3 conditions: cine-MR at the isocenter (0 cm offset) for 5 time points, continuous measurement at the isocenter, and continuous measurement 10cm offset from the isocenter. CFD simulation was performed on commercial software COMSOL. Image post-processing was done using in-house Python tools. Qualitative comparisons were made using Paraview while quantitative comparisons were assessed by correlation and Bland-Altman plots.

**Results:** Imaging at 10 cm from isocenter was found to adequately visualize secondary flows such as jets in the aneurysm. Total flow through the inlets obtained from the 2D- and 4D- MRV acquisitions were  $4.03 \pm 0.07$  mL/s and  $3.65 \pm 0.12$  mL/s, which were significantly larger than the directly measured flow of 3.1 mL/s. The overall velocity field from the CFD results underestimate the measurements from 4D MRV, suggesting they provided inlet boundary

conditions are too low. The greatest differences between the CFD and 4D MRV results appear at the vessel walls.

**Conclusion:** We developed a pipeline for evaluating flow measured under different conditions and modalities. A combination of noise and partial volume effects compromise velocity measurements, particularly in voxels at the vessel edge. Additionally, CFD can provide precise measurements at the wall, but the accuracy of the results depends highly on the image-derived geometric and flow boundary conditions.

## Table of Contents

Chapter 1	Introduction . . . . .	1
Chapter 2	Materials and methods . . . . .	4
Chapter 3	Results . . . . .	10
Chapter 4	Discussions . . . . .	16
Chapter 5	References . . . . .	19
Chapter 6	Publishing Agreement . . . . .	25

## List of tables

Table 1	Flow rate of 2D MRV and 4D MRV . . . . .	13
---------	--	----



**List of Figures**

Figure 1 Flow phantom and flow system set-up . . . . . 5

Figure 2 Illustrations of flow system setup and details in MR scanning . . . . . 7

Figure 3 Comparison of the velocity streamlines of 0 cm offset (left) and 10 cm offset  
(right) in the intracranial aneurysm . . . . . 10

Figure 4 Comparison of flow along inlet vessels for following conditions. . . . . 12

Figure 5 Comparison of the velocity field between 4D MRV and CFD . . . . . 15

## **Introduction**

Knowledge of blood flow patterns in the human body is a critical component in cardiovascular disease research and diagnosis. Two different approaches to flow assessment are currently available to the researcher and clinician: direct model-independent velocity mapping using phase contrast magnetic resonance imaging (PC-MRI) (1, 2) or Doppler ultrasound; and model-based computational fluid dynamics (CFD) calculations (3-15). Compared to Doppler ultrasound, PC-MRI has gained prominence in recent years due to its unrestricted 3D anatomical coverage, minimal operator dependence, and ability to directly measure 3D velocity maps (16).

Magnetic Resonance Velocimetry (MRV) is a method to obtain velocity fields in the human vascular system. The velocities are usually obtained with PC-MRI techniques using special gradient waveforms. Alternatively, vascular flow can be estimated from model-based CFD calculations. CFD is a branch of fluid mechanics that uses computational methods to solve and analyze problems that involve fluid flows. Numerical simulations are performed to solve the interaction of liquids with surfaces defined by geometric and inlet flow boundary conditions.

In general, MRV directly accounts for actual physiological flows such as turbulence, compliance and non-Newtonian flow – factors that are poorly accounted for by CFD. On the other hand, CFD is a powerful tool for describing flow fields in both idealized models and patient specific geometries (17). CFD provides extremely high resolution, but its accuracy depends on model assumptions and accurate boundary conditions while velocity fields measured with PC-MRI generally do not automatically agree with the equations of fluid dynamics, provide limited resolution, suffer from intrinsic acquisition noise, and partial volume effects (18).

Recently, MRV has been applied to the evaluation of congenital heart disease (CHD), the thoracic aorta, hepatic and portal venous flow, pulmonary arteries, renal arteries, carotid arteries and intracranial hemodynamics. A number of groups have shown that 4D flow MRI can be used to derive advanced hemodynamic measures such as wall shear stress (WSS) (19-21), pressure difference (22-25), pulse wave velocity (26, 27), turbulent kinetic energy (TKE) and others (28, 29) for an improved characterization of cardiovascular disease beyond simple measures of flow. Such parameters can be used to evaluate patient health and inform surgical decisions as clinical applications.

Previously several in vitro studies have been performed to validate results predicted using numerical simulation methods (3-15). Previous experiments compared the blood flow simulation results to physical measurements acquired using techniques such as laser Doppler anemometry and PC-MRI. While these experiments produced favorable results, they were limited in scope. They looked at simpler geometries, such as idealized bifurcations (30, 31) or anastomotic junctions (32). These validation studies relied on a priori knowledge of the flow distribution, information that is not available for surgical simulation problems. Furthermore, the flow conditions in these experiments were less complex than those found in large arteries in vivo.

PC-MRI is susceptible to unique artifacts that may alter the qualitative visualization of flow, and introduce errors in the velocimetry. There is no single dominant source of error, however several smaller errors may accumulate and result in velocity or flow measurement errors on the order of 5 % to 10 % or more. It is important to note that the relative importance of different sources of artifact depends on the type of measurement being made, e.g., peak velocity or volume flow, and the type of pulse sequence being used (33).

The velocity distortion is noted in phase difference images, notably from gradient eddy current effects (34), concomitant field (i.e., Maxwell) terms (35), and gradient field distortions (36). Such phase offset errors are thought to exhibit a substantial increase with increasing distance from the isocenter of the MR system, with the concomitant field and gradient field distortion in particular varying super-linearly with distance. Even small systematic inaccuracies in measured velocity can propagate into larger errors when computing volume flow. Its consequence and corrections have been reported in previous studies (36-38).

In a study by Choudhri et al. (39), spatial distortion was noted and was felt to be related to head positioning relative to the isocenter of the magnetic field during preoperative localization MRI. In this study, the images obtained after repositioning the head closer to the isocenter of the magnetic field showed less distortion than the initial scan performed away from the isocenter without and with application of the manufacturer's distortion correction algorithm. This result indicates that in-scanner distortion correction algorithms decreased the degree of distortion, but were not as accurate as scans performed closer to the isocenter of the scanner. Image reconstruction assumes a uniform  $B_0$  over the field of view. If the patient is located too far from the isocenter, some parts of the field of view enter the fringe field and experience decreased  $B_0$ . As a result, the Larmor frequency of protons in that area is decreased; as field variations are assumed to be due to gradient coils, reconstruction displaces the signal obtained along the frequency-encoding direction. However, whether it can be applied to the flow imaging or how much flow distortion will remain uncorrected remains unknown.

To address these problems, our goal is to develop and use a fast and reproducible model flow system with a highly structured velocity field that can be used to assess the accuracy of various

features of MRV, and then compare MRV results to CFD simulations. In this study, we investigated the reproducibility of the measurements by comparing results from 2D MRV, 4D MRV and CFD. We also investigated the sensitivity of the measurements, which could be affected by effects such as gradient field imperfections, to positional variation in the scanner.

## **Materials and methods**

### **Pumping system setup**

The pumping system setup consisted of a flow phantom and a pressure-head driven flow system. The flow phantom is a life-sized replica of an intracranial aneurysm imaged from a patient (Figure 1a). In order to reduce the setup time associated with a previous cumbersome flow system in the laboratory, a new simpler plastic-based system was designed. Flow is generated between two cubic reservoirs at different heights, and under idealized conditions, the velocity depends on the height difference of the two cubes as follows:

$$\frac{1}{2}mv^2 = mgh_1 - mgh_2 \quad (1)$$

$$\frac{1}{2}mv^2 = mg\Delta h \quad (2)$$

$$v = \sqrt{2g\Delta h} \quad (3)$$

where  $m$  is the mass of the fluid,  $g$  is the gravitational constant,  $h_1$  is height of the higher cube,  $h_2$  is height of the lower cube, and  $\Delta h$  is the height difference between the cubes.

The main idea is to provide steady flow in terms of the height difference from Eq. 3. Two hollow cubes were designed with mechanical design software (Autodesk Inventor 2016) and then printed out in Poly-Lactic Acid (PLA) material using a 3D printer (2014 Type A Machines Series 1, Figure 1c).

The flow system consists of two hollow cubes, an aneurysm phantom, a reservoir for overflow from each cube that was filled with 4L water, an air pump, and MR-compatible tubes and connectors (Figure 1b and Figure 2a). In operation the pump replenished the upper cube sufficiently that it overflowed with an overflow channel back to the reservoir. All flow into the lower cube similarly overflowed into an overflow channel and returned to the reservoir. The flow system was assembled in the MRI scanner room. Before scanning, the flow rate was determined by performing volume collection in a graduated cylinder for 100 seconds establishing ground truth for the volume flow rate.

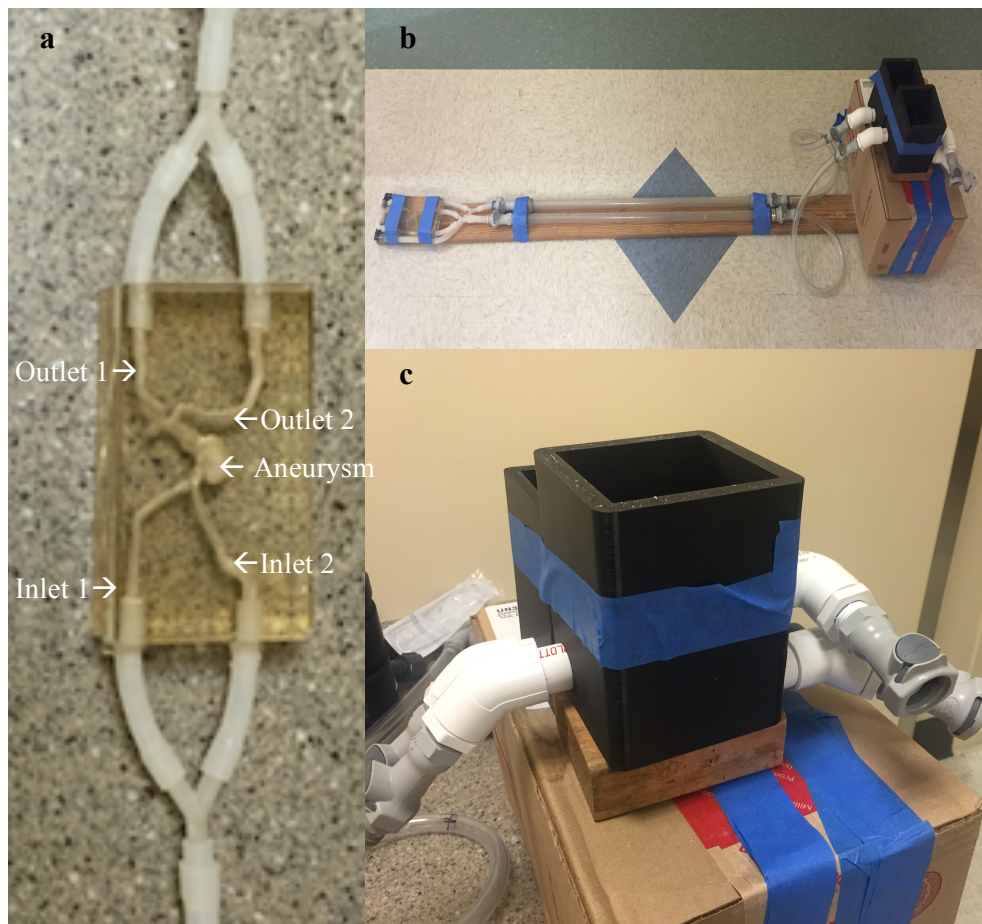


**Figure 1. Flow phantom and flow system set-up.** a) The phantom of the intracranial aneurysm. Five landmarks depict inlet 1, inlet 2, aneurysm, outlet 1 and outlet 2, b) flow system setup, and c) two black hollow cubes printed by the 3D printer with supply channels, channels into and out of the aneurysm segment, and overflow channels.

## MR imaging

In order to apply background correction in the post-processing stage, saline bags were wrapped around the flow phantom before MR scanning. All MR images of the model were obtained on a 3T Siemens MAGNETOM Skyra MRI scanner (Siemens Healthcare, Erlangen, Germany) using two small element coils, one anterior and one posterior. A 2D gradient-echo sequence was used for localizing the aneurysm and followed by a higher resolution 3D MRA that covered the whole phantom. The acquisition parameters were as follows: TR/TE = 4.43/1.84 ms, flip angle (FA) = 20°, field of view (FOV) =  $224 \times 182 \times 60 \text{ mm}^3$ , voxel size =  $0.5 \times 0.5 \times 0.5 \text{ mm}^3$ , receiver bandwidth = 505 Hz/pixel, and number of averages (NA) = 1.

Next, the phantom was scanned using 4D MRV under 3 conditions: cine PC-MRV at 0 cm offset using a dummy cardiac pulse every 500 ms and with 5 time points within each pulse cycle (velocity encoding (VENC) = 50 cm/s, TR/TE = 84.96/4.2 ms, FA = 12°, FOV =  $240 \times 180 \times 130 \text{ mm}^3$ , voxel size =  $1.25 \times 1.25 \times 1.25 \text{ mm}^3$  receiver bandwidth = 400 Hz/pixel, NA = 1), continuous PC-MRV at the isocenter and 10 cm offset from the isocenter, namely, moving the table 10 cm out (Figure 2b). Other than the number of phases, acquisition parameters were the same in continuous PC-MRV as in cine PC-MRV.

2D MRV of through-plane blood flow velocities in the two inlet vessels were measured 3 cm below the aneurysm. The sagittal and coronal projections (MIP) of the 2D gradient-echo scan

were used to position the imaging slice transverse to the vessel of the interest. For each inlet vessel, 2D MRV images were acquired in 5 sequential positions at 2 mm intervals. Additionally, one image at the distal convergence of the aneurysm was acquired to measure the total flow (Figure 2c). The acquisition parameters were: VENC = 50 cm/s, TR/TE = 41.52/4.26 ms, FA = 20°, FOV = 200 × 200 mm<sup>2</sup>, slice thickness = 5 mm voxel size = 0.83 × 0.83 mm<sup>2</sup>, receiver bandwidth = 495 Hz/pixel, NA = 1.

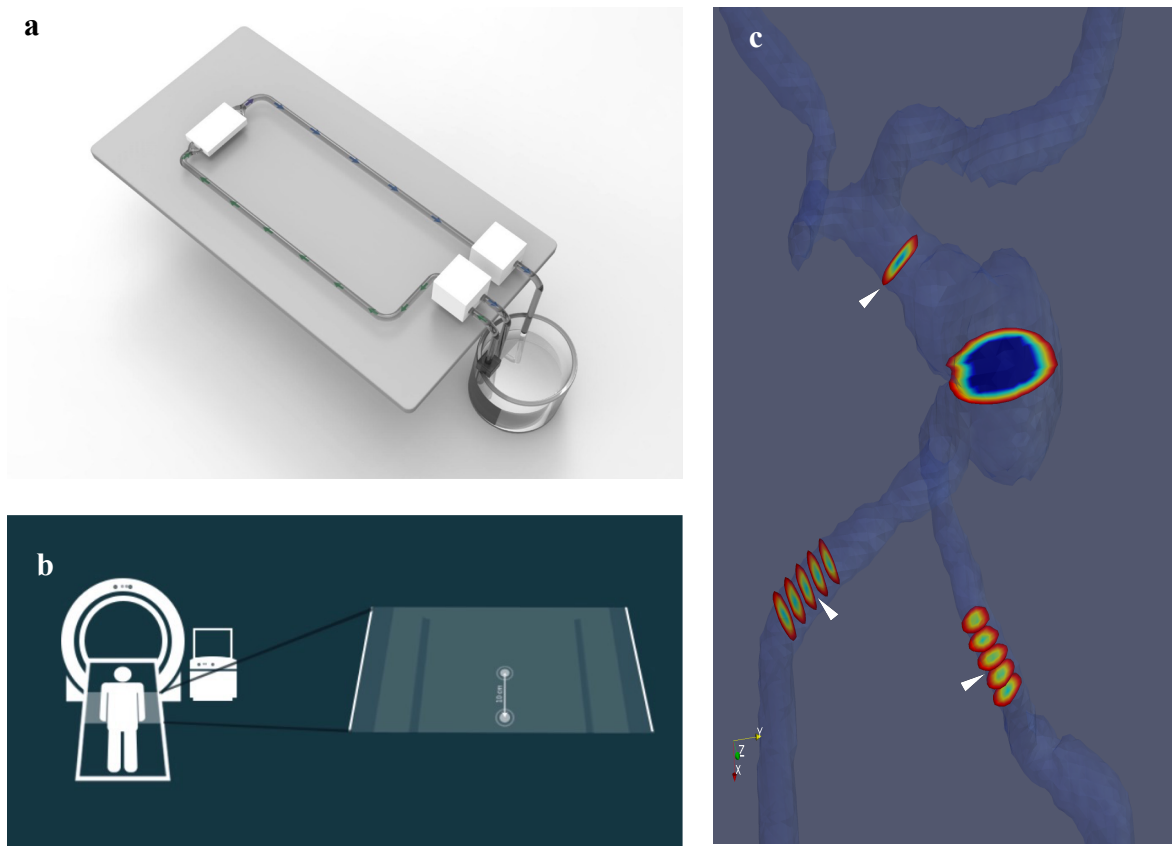


**Figure 2. Illustrations of flow system setup and details in MR scanning.** a) A schematic of the flow system setup, b) the flow phantom was scanned at 2 positions: first at the isocenter then 10 cm towards the inferior direction, and c) an illustration of planes imaged in 2D MRV: 5 planes for both inlet 1 and inlet 2, one plane for distal aneurysm (arrowheads).



## **Flow Quantification and comparisons**

Images were post-processed using in-house tools developed with Python and the PyQt, VTK, VMTK, and SciPy packages. For each image set, semi-automated segmentation of the 3D MRA was performed on an in-house tool to obtain a 3D iso-surface defining the intra-luminal volume of the aneurysm. The main idea of segmentation involved lofting together contours based on a series of 2D level set segmentations along each vessel. Eddy current induced background phase errors were determined from a linear fit of the static tissue and were subsequently subtracted from the velocity maps. Both the imaging and simulation results were qualitatively compared by viewing the streamlines and velocity fields in Paraview. Comparisons between 4D MR velocity measurements under different conditions were performed using point-wise comparisons of the velocity components. 5 phases in cine MRV were averaged to improve the statistics of the measurement. These comparisons were visualized by correlation and Bland-Altman plots. Due to geometry distortion, and to perform point-wise comparisons between 0cm-offset and 10cm-offset geometries, the former was registered into the latter using a combination of registration, geometry transformation, and data interpolation filters in Paraview. This method assumes that no changes occurred in the length of the vessels, a fair assumption based on extensive phantom experience in aneurysm assessment. Similarly, data from the CFD simulation was compared to the 4D MRV by interpolating the 4D MRV measurements at the CFD mesh points. To compare 2D and 4D MRV results, vascular lumen cross-sections were obtained along the vessel centerline at 2 mm intervals, and cross-sectional areas were calculated. Flow from the 4D image data was obtained at five planes corresponding to the 2D MRV positions for each inlet. Also, flow through one plane at the distal part of the aneurysm was obtained to compare the total flow rate.

## **CFD simulation**

The geometry for the simulation was obtained by segmentation of the aneurysm on the MRA images with in-house python tools and Paraview (Version 5.1.0 64-bit). The resulting 3D iso-surface defining the intra-luminal volume of the aneurysm was edited in Geomagic Design X. In order to avoid flow entrance effects, a section of the vessel segment proximal to the aneurysm was included in all CFD models. The total flow for the inlet boundary conditions was obtained from the experiment measurement. The ratio of the flow between the two inlets was estimated using the flows measured from the cine MR acquisition. Tetrahedral mesh generation and simulation were performed in COMSOL, which uses a finite element approach to solve the Navier-Stokes equations. A steady flow simulation was conducted on subsequently refined meshes. To specify the inlet velocity, the cross sectional area of two inlets were measured. The outlet pressure was set to zero.

The flow was assumed to be Newtonian flow with the viscosity of water in all simulations. The walls of the aneurysm and vessels were considered to be rigid. Non-Newtonian blood behavior is crucial only when the size of the vessel is comparable to the size of red blood cells or in regions with low shear stress, neither of which is relevant to the case of this phantom.

## Results

### Comparisons of velocity at different positions

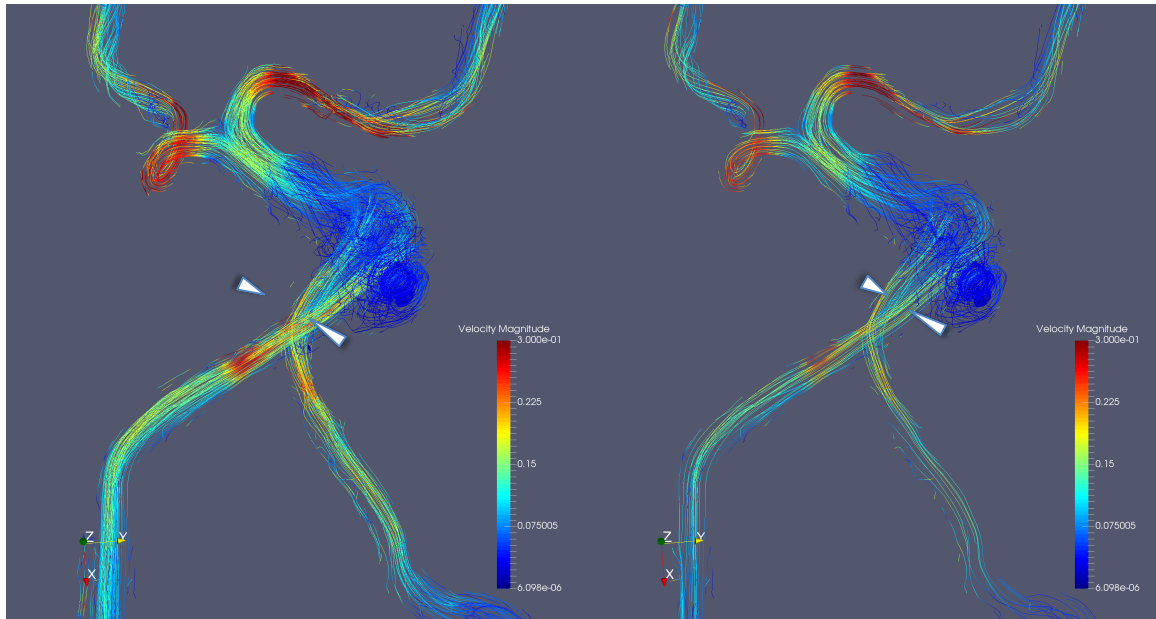


**Figure 3. Comparison of the velocity streamlines of 0 cm offset (left) and 10 cm offset (right) in the intracranial aneurysm phantom with two jets in the inlet flow (arrows).**

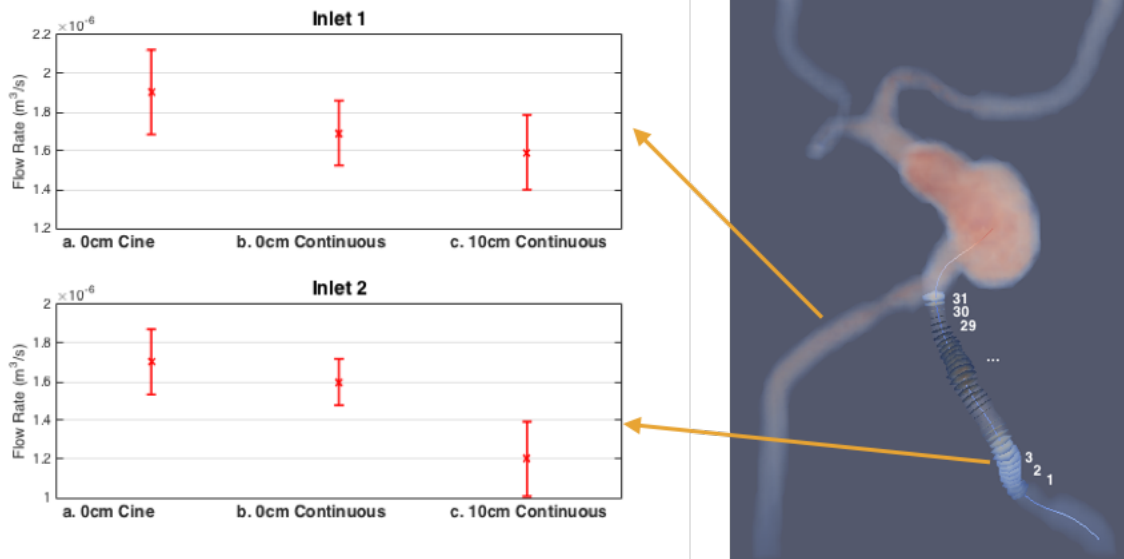
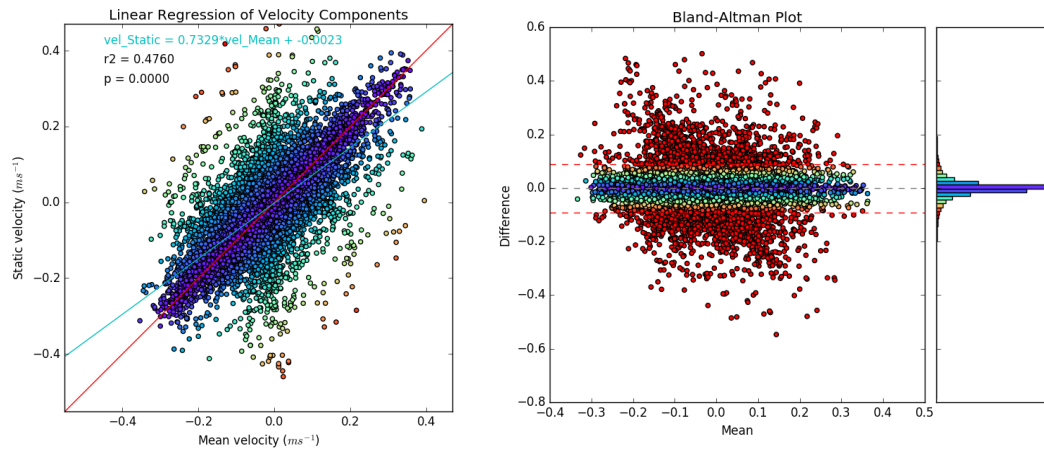
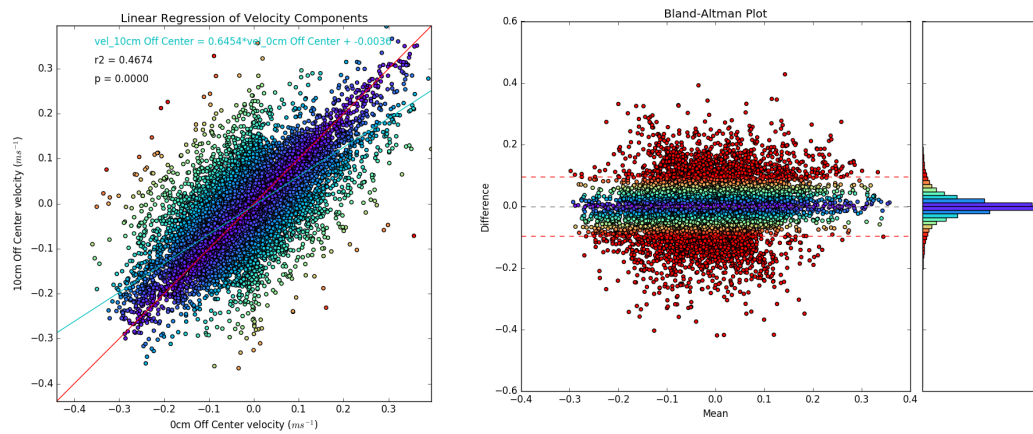
The streamlines at 0 cm offset and 10 cm offset were generated with Paraview. Both imaging at 0 cm and 10 cm offset from the isocenter adequately visualized the major flow features such as the jets in the aneurysm. The streamlines are similar apart from the slightly lower bulk flow imaging at 10 cm offset compared to imaging at 0 cm offset (Figure 3).

### Comparison of flow along inlet vessels under 3 conditions

31 Vascular lumen cross-sections were obtained along the vessel centerline at 1 mm intervals at the region proximal to the aneurysm and the flow rate of each slice were calculated in Paraview. As shown in the Figure 4A, the mean velocity of cine MRV and continuous MRV at two inlets

are more similar than that of 10 cm offset continuous imaging condition. The flow rate in a, b, c conditions are  $1.90 \pm 0.22$  mL/s,  $1.69 \pm 0.17$  mL/s,  $1.59 \pm 0.19$  mL/s and  $1.70 \pm 0.17$  mL/s,  $1.60 \pm 0.12$  mL/s,  $1.20 \pm 0.19$  mL/s respectively for inlet 1 and inlet 2.

From Figure 4B and 4C, both have good correlations and  $r^2$  is 0.4760 and 0.4674 respectively. The linear regression curves are close to the orthogonal curves. The closer of two curves corresponds to the closer mean velocity of two measurements. The significant scatter is considered to originate from noise in the images, particularly from edge voxels. From the Bland-Altman plot most data points concentrate close to zero difference, indicating good agreement in both the cine vs. continuous MR at 0 cm offset and 10 cm offset.

**A****B****C**

**Figure 4. Comparison of flow along inlet vessels under different conditions.** A) For each of two inlets: a. time-average of 5 cine measurements at 0 cm offset; b. continuous measurements at 0 cm offset; c. continuous measurements at 10 cm offset. Linear regression of velocity components and Bland-Altman plot are shown in B) cine vs. continuous at 0 cm offset and C) cine vs. continuous at 10 cm offset. In the correlation, the red line represents perfect agreement whereas the green line is the linear regression curve. In the Bland-Altman plot, the dashed curves are twice the standard deviation of the point-wise difference between two datasets.

**Table 1.** Flow rate of 2D MRV and 4D MRV

	<b>2D MRV (mL/s)</b>	<b>4D MRV (mL/s)</b>
<b>Inlet 1</b>	1.95 ± 0.09	2.04 ± 0.06
<b>Inlet 2</b>	2.07 ± 0.11	1.60 ± 0.13
<b>Total</b>	4.03 ± 0.07	3.64 ± 0.12
<b>Distal</b>	3.21	3.38

Total flow through the inlets obtained from the 2D- and 4D- MRV acquisitions were  $4.03 \pm 0.07$  mL/s and  $3.65 \pm 0.12$  mL/s (Table 1), which are significantly larger than the directly measured flow of 3.1 mL/s. The relatively low standard deviations suggest systematic errors, such as scanner mis-calibration or incorrect segmentations, are responsible for the discrepancies rather than noise alone. The flow rate measured at the distal slice of the aneurysm in 2D and 4D MRV were 3.21 mL/s and 3.38 mL/s respectively (Table 1), which could be related to the larger caliber of the vessel at that location.

### **Comparison of CFD and 4D MRV**

Velocity magnitudes from the numerical simulations are mapped. From Figure 5a and 5b, the overall velocity field from the CFD results appears to underestimate the measurements from 4D MRV, suggesting that the provided inlet boundary conditions are too low, which is also shown in Figure 5c. The largest differences between the CFD and 4D MRV results appear at the vessel walls, which are physically and computationally subject to the no-slip condition, but are most vulnerable to noise and partial volume effects (Figure 5c). Also, in Figure 5d, the points where CFD velocity is close to zero correspond to a large variation of 4D MRV, further demonstrating the effects of noise and partial volume of the edge voxels.

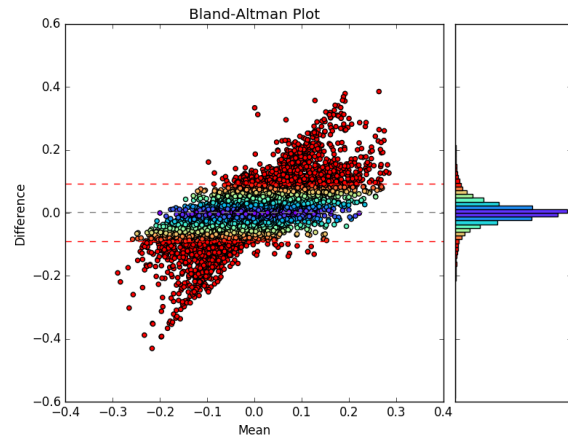
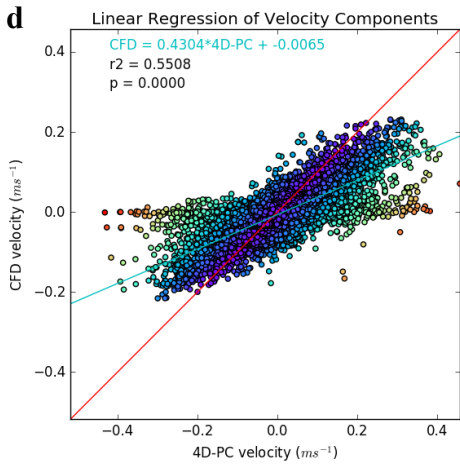
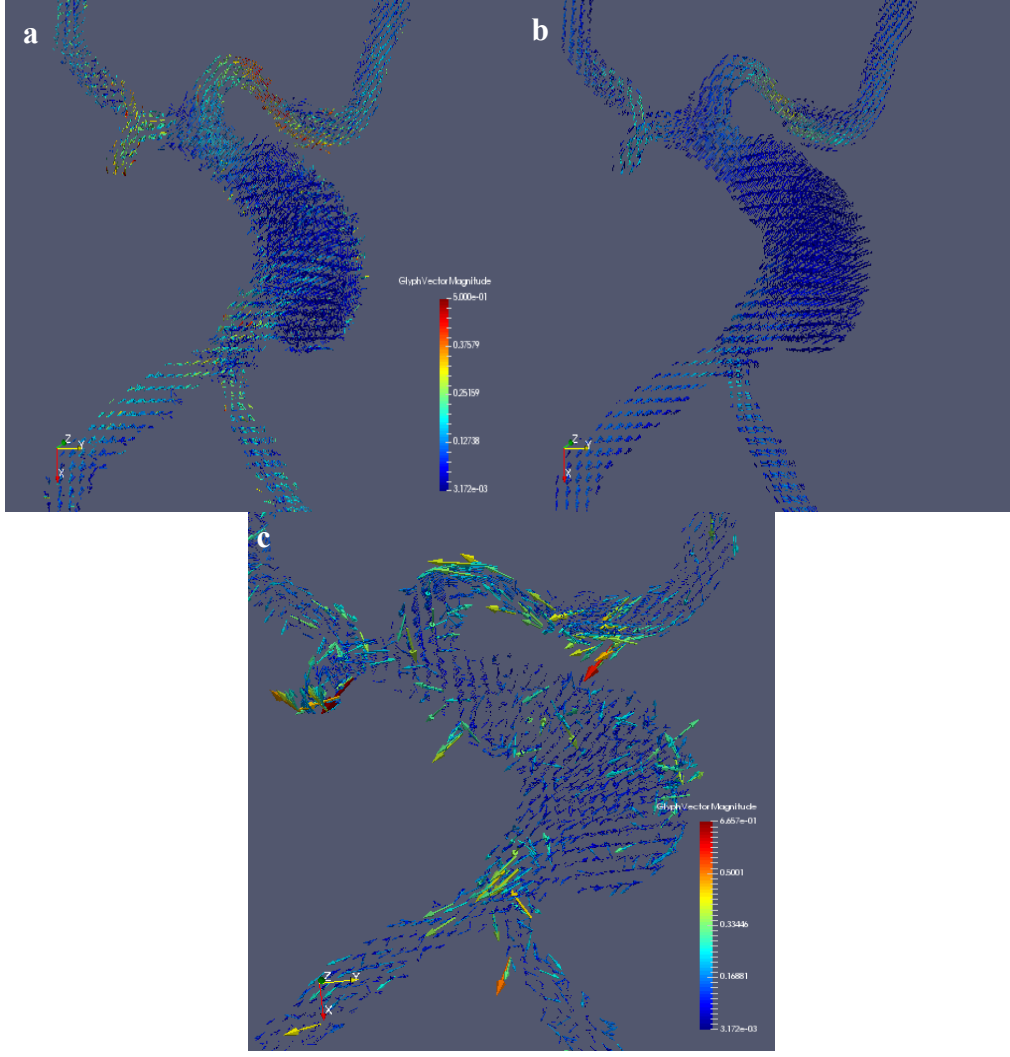




**Figure 5. Comparison of the velocity field between a) 4D MRV and b) CFD.** The difference of velocity field of 4D MRV and CFD is shown in c) and the Correlation and Bland-Altman plots between them are displayed in d).

## **Discussion**

Velocity offsets in MRV flow assessment is a long-standing known problem. Three major sources of inaccuracy in velocity images include eddy current effects, Maxwell terms and gradient field non-linearities. In the study by Gatehouse et al. (37), none of the tested CMR systems remained consistently below the proposed maximum acceptable offset of 0.6 cm/s, which is thought to be an acceptable error for estimating average cardiac output. For our study, this value is expected to be even lower as the phantom is in the intracranial region. Thus, additional actions are necessary for achieving reliable MRV measurements. Possible additional measurements can be divided into two categories: 1. reduction of offsets by sequence optimization and 2. correction of the acquired images by post-processing with or without a separate phantom scan (41).

In our study, we used stationary saline bags wrapping around the phantom so as to provide a baseline reference for zero velocity. This method is developed by Walker et al. (34). Any nonzero velocity in the stationary tissue represents a baseline offset error, whose magnitude is used to correct the flow in the vessel in the post-processing. Basically, this method corrects for distortion from eddy currents, which is a user interaction that is always required. Maxwell terms are generally automatically corrected before image reconstruction by the MR system and gradient field distortions can also be corrected for a given gradient field model.

We found that the flow measurement in both 2D MRV and 4D MRV have noticeable errors ( $4.03 \pm 0.07$  mL/s and  $3.64 \pm 0.12$  mL/s compared to ground truth 3.10 mL/s) but this is reduced for flow measured distal to the aneurysm (3.21 mL/s and 3.38 mL/s). This is likely due to greater errors from the edge voxels of small vessels. In larger vessels, more accurate flow measurements were obtained due to larger number of voxels at the edges and less segmentation errors. The accuracy of flow measurement by MRV needs to be further validated and if necessary, gradient field non-linearity correction should be applied during image reconstruction.

It is thought that flow measurement errors increase substantially with increasing distance from the isocenter of the MR system. For each inlet, velocity and flow rate are slightly lower at 10 cm offset than 0 cm offset due to non-linear gradient fields and post-processing errors. Further study needs to be done to validate the results at 10 cm offset and to explore how additional offsets (e.g. 20 cm offset, other directions of offset) might further impact the results given that many clinical applications require a broader FOV covering.

The  $r^2$  of correlation of continuous 0 cm and 10 cm offset to the cine ground truth (0.4760 and 0.4674) shows that almost half of the variabilities are not around its mean value. This may result from there being only 2-3 pixels per cross-section in the inlet vessel and severe partial volume effects due to limited isotropic 1.3 mm resolution. To obtain a flow error of less than 10% or 5%, it is suggested that the vessel should be at least 4 or 5 pixels in diameter (42). Apart from partial volume errors, other systematic errors include intravoxel phase dispersion, velocity aliasing and imaging plane misalignment (43).

CFD simulations can provide information at the boundaries where 4D MRV is noisiest. CFD

simulation assumes zero velocity at the boundary of vessel walls, which is called the no-slip condition. Although partial volume effects compromise the velocity and flow measurement of 4D MRV, one previous study showed that by including partial volumed edge pixels in vessel segmentation, less error was produced than when excluding them in numerical simulations. For CFD simulation, the geometry and boundary conditions are dependent on the MRA and MRV data. Obtaining accurate flow measurements requires an excellent estimate of the boundary of the vessel and sufficient SNR in the magnitude image (42), which, in this study, could be the reason for errors from CFD simulation. Further study is required to validate that the overall velocity field from the CFD simulation matches 4D MRV measurement.

We therefore conclude that this project provided a flow model with highly structured flow that could be used as part of an evaluation pipeline for comparing flow measurements under different conditions, and on different scanners. Systematic noise and partial volume effects compromise the velocity and flow measurements at the edge voxels of vessels. In addition, post-processing such as segmentation also needs to be carefully performed to provide accurate measurements. In turn, CFD can provide precise measurements at the wall of vessels where 4D MRV is noisiest. However, due to similar noise issues, especially in lumens of small diameter, the accuracy of the results depends highly on the image-derived geometric and inlet boundary conditions.

## References

- 1 Pelc NJ, Herfkens RJ, Shimakawa A, Enzmann DR. Phase contrast cine magnetic resonance imaging. *Magnetic resonance quarterly*. 1991 Oct;**7**(4):229-54.
- 2 Sigfridsson A, Petersson S, Carlhall CJ, Ebbers T. Four-dimensional flow MRI using spiral acquisition. *Magnetic resonance in medicine*. 2012 Oct;**68**(4):1065-73.
- 3 Steinman DA, Taylor CA. Flow imaging and computing: large artery hemodynamics. *Annals of biomedical engineering*. 2005 Dec;**33**(12):1704-9.
- 4 Giddens DP, Zarins CK, Glagov S. The role of fluid mechanics in the localization and detection of atherosclerosis. *Journal of biomechanical engineering*. 1993 Nov;**115**(4B):588-94.
- 5 Steinman DA. Image-based computational fluid dynamics: a new paradigm for monitoring hemodynamics and atherosclerosis. *Current drug targets Cardiovascular & haematological disorders*. 2004 Jun;**4**(2):183-97.
- 6 Lei M, Kleinstreuer C, Truskey GA. Numerical investigation and prediction of atherogenic sites in branching arteries. *Journal of biomechanical engineering*. 1995 Aug;**117**(3):350-7.
- 7 Hyun S, Kleinstreuer C, Archie JP, Jr. Hemodynamics analyses of arterial expansions with implications to thrombosis and restenosis. *Medical engineering & physics*. 2000 Jan;**22**(1):13-27.
- 8 Long Q, Xu XY, Ariff B, Thom SA, Hughes AD, Stanton AV. Reconstruction of blood flow patterns in a human carotid bifurcation: a combined CFD and MRI study. *Journal of magnetic resonance imaging : JMRI*. 2000 Mar;**11**(3):299-311.
- 9 Worth Longest P, Kleinstreuer C. Comparison of blood particle deposition models for non-parallel flow domains. *Journal of biomechanics*. 2003 Mar;**36**(3):421-30.
- 10 Boussel L, Rayz V, Martin A, et al. Phase-contrast magnetic resonance imaging measurements in intracranial aneurysms in vivo of flow patterns, velocity fields, and wall shear

stress: comparison with computational fluid dynamics. *Magnetic resonance in medicine*. 2009 Feb;**61**(2):409-17.

11 Canstein C, Cachot P, Faust A, et al. 3D MR flow analysis in realistic rapid-prototyping model systems of the thoracic aorta: comparison with in vivo data and computational fluid dynamics in identical vessel geometries. *Magnetic resonance in medicine*. 2008 Mar;**59**(3):535-46.

12 Milner JS, Moore JA, Rutt BK, Steinman DA. Hemodynamics of human carotid artery bifurcations: computational studies with models reconstructed from magnetic resonance imaging of normal subjects. *Journal of vascular surgery*. 1998 Jul;**28**(1):143-56.

13 Papathanasopoulou P, Zhao S, Kohler U, et al. MRI measurement of time-resolved wall shear stress vectors in a carotid bifurcation model, and comparison with CFD predictions. *Journal of magnetic resonance imaging : JMRI*. 2003 Feb;**17**(2):153-62.

14 Thomas JB, Milner JS, Rutt BK, Steinman DA. Reproducibility of image-based computational fluid dynamics models of the human carotid bifurcation. *Annals of biomedical engineering*. 2003 Feb;**31**(2):132-41.

15 Marshall I, Zhao S, Papathanasopoulou P, Hoskins P, Xu Y. MRI and CFD studies of pulsatile flow in healthy and stenosed carotid bifurcation models. *Journal of biomechanics*. 2004 May;**37**(5):679-87.

16 Rispoli VC, Nielsen JF, Nayak KS, Carvalho JL. Computational fluid dynamics simulations of blood flow regularized by 3D phase contrast MRI. *Biomedical engineering online*. 2015;**14**(1):110.

17 Sigovan M, Rayz V, Gasper W, Alley HF, Owens CD, Saloner D. Vascular remodeling in autogenous arterio-venous fistulas by MRI and CFD. *Annals of biomedical engineering*. 2013 Apr;**41**(4):657-68.

- 18 Stankovic Z, Allen BD, Garcia J, Jarvis KB, Markl M. 4D flow imaging with MRI. Cardiovascular diagnosis and therapy. 2014 Apr;**4**(2):173-92.
- 19 Stalder AF, Russe MF, Frydrychowicz A, Bock J, Hennig J, Markl M. Quantitative 2D and 3D phase contrast MRI: optimized analysis of blood flow and vessel wall parameters. Magnetic resonance in medicine. 2008 Nov;**60**(5):1218-31.
- 20 Markl M, Wallis W, Harloff A. Reproducibility of flow and wall shear stress analysis using flow-sensitive four-dimensional MRI. Journal of magnetic resonance imaging : JMRI. 2011 Apr;**33**(4):988-94.
- 21 Oshinski JN, Curtin JL, Loth F. Mean-average wall shear stress measurements in the common carotid artery. Journal of cardiovascular magnetic resonance : official journal of the Society for Cardiovascular Magnetic Resonance. 2006;**8**(5):717-22.
- 22 Bock J, Frydrychowicz A, Lorenz R, et al. In vivo noninvasive 4D pressure difference mapping in the human aorta: phantom comparison and application in healthy volunteers and patients. Magnetic resonance in medicine. 2011 Oct;**66**(4):1079-88.
- 23 Tyszka JM, Laidlaw DH, Asa JW, Silverman JM. Three-dimensional, time-resolved (4D) relative pressure mapping using magnetic resonance imaging. Journal of magnetic resonance imaging : JMRI. 2000 Aug;**12**(2):321-9.
- 24 Ebbers T, Wigstrom L, Bolger AF, Engvall J, Karlsson M. Estimation of relative cardiovascular pressures using time-resolved three-dimensional phase contrast MRI. Magnetic resonance in medicine. 2001 May;**45**(5):872-9.
- 25 Lum DP, Johnson KM, Paul RK, et al. Transstenotic pressure gradients: measurement in swine--retrospectively ECG-gated 3D phase-contrast MR angiography versus endovascular pressure-sensing guidewires. Radiology. 2007 Dec;**245**(3):751-60.

- 26 Bolster BD, Jr., Atalar E, Hardy CJ, McVeigh ER. Accuracy of arterial pulse-wave velocity measurement using MR. *Journal of magnetic resonance imaging : JMRI*. 1998 Jul-Aug;**8**(4):878-88.
- 27 Markl M, Wallis W, Brendecke S, Simon J, Frydrychowicz A, Harloff A. Estimation of global aortic pulse wave velocity by flow-sensitive 4D MRI. *Magnetic resonance in medicine*. 2010 Jun;**63**(6):1575-82.
- 28 Dyverfeldt P, Sigfridsson A, Kvitting JP, Ebbers T. Quantification of intravoxel velocity standard deviation and turbulence intensity by generalizing phase-contrast MRI. *Magnetic resonance in medicine*. 2006 Oct;**56**(4):850-8.
- 29 Dyverfeldt P, Gardhagen R, Sigfridsson A, Karlsson M, Ebbers T. On MRI turbulence quantification. *Magnetic resonance imaging*. 2009 Sep;**27**(7):913-22.
- 30 Gijssen FJ, van de Vosse FN, Janssen JD. The influence of the non-Newtonian properties of blood on the flow in large arteries: steady flow in a carotid bifurcation model. *Journal of biomechanics*. 1999 Jun;**32**(6):601-8.
- 31 Perktold K, Hofer M, Rappitsch G, Loew M, Kuban BD, Friedman MH. Validated computation of physiologic flow in a realistic coronary artery branch. *Journal of biomechanics*. 1998 Mar;**31**(3):217-28.
- 32 Papaharilaou Y, Doorly DJ, Sherwin SJ. Assessing the accuracy of two-dimensional phase-contrast MRI measurements of complex unsteady flows. *Journal of magnetic resonance imaging : JMRI*. 2001 Dec;**14**(6):714-23.
- 33 Nayak KS, Nielsen JF, Bernstein MA, et al. Cardiovascular magnetic resonance phase contrast imaging. *Journal of cardiovascular magnetic resonance : official journal of the Society for Cardiovascular Magnetic Resonance*. 2015;**17**:71.

- 34 Walker PG, Cranney GB, Scheidegger MB, Waseleski G, Pohost GM, Yoganathan AP. Semiautomated method for noise reduction and background phase error correction in MR phase velocity data. *Journal of magnetic resonance imaging : JMRI*. 1993 May-Jun;**3**(3):521-30.
- 35 Bernstein MA, Zhou XJ, Polzin JA, et al. Concomitant gradient terms in phase contrast MR: analysis and correction. *Magnetic resonance in medicine*. 1998 Feb;**39**(2):300-8.
- 36 Chernobelsky A, Shubayev O, Comeau CR, Wolff SD. Baseline correction of phase contrast images improves quantification of blood flow in the great vessels. *Journal of cardiovascular magnetic resonance : official journal of the Society for Cardiovascular Magnetic Resonance*. 2007;**9**(4):681-5.
- 37 Gatehouse PD, Rolf MP, Graves MJ, et al. Flow measurement by cardiovascular magnetic resonance: a multi-centre multi-vendor study of background phase offset errors that can compromise the accuracy of derived regurgitant or shunt flow measurements. *Journal of cardiovascular magnetic resonance : official journal of the Society for Cardiovascular Magnetic Resonance*. 2010;**12**:5.
- 38 Holland BJ, Printz BF, Lai WW. Baseline correction of phase-contrast images in congenital cardiovascular magnetic resonance. *Journal of cardiovascular magnetic resonance : official journal of the Society for Cardiovascular Magnetic Resonance*. 2010;**12**:11.
- 39 Choudhri AF, Chin EM, Klimo P, Boop FA. Spatial distortion due to field inhomogeneity in 3.0 tesla intraoperative MRI. *The neuroradiology journal*. 2014 Sep;**27**(4):387-92.
- 40 Ku JP, Draney MT, Arko FR, et al. In vivo validation of numerical prediction of blood flow in arterial bypass grafts. *Annals of biomedical engineering*. 2002 Jun;**30**(6):743-52.
- 41 Rolf, M. P., et al. (2011). Sequence optimization to reduce velocity offsets in cardiovascular magnetic resonance volume flow quantification--a multi-vendor study. *J Cardiovasc Man Reson* **13**: 18.



42 Jiang, J., et al. (2015). "Quantifying errors in flow measurement using phase contrast magnetic resonance imaging: comparison of several boundary detection methods." *Magn Reson Imaging* **33**(2): 185-193.


43 Wolf, R. L., et al. (1993). "Analysis of systematic and random error in MR volumetric flow measurements." *Magn Reson Med* **30**(1): 82-91

**Publishing Agreement**

*It is the policy of the University to encourage the distribution of all theses, dissertations, and manuscripts. Copies of all UCSF theses, dissertations, and manuscripts will be routed to the library via the Graduate Division. The library will make all theses, dissertations, and manuscripts accessible to the public and will preserve these to the best of their abilities, in perpetuity.*

**Please sign the following statement:**

*I hereby grant permission to the Graduate Division of the University of California, San Francisco to release copies of my thesis, dissertation, or manuscript to the Campus Library to provide access and preservation, in whole or in part, in perpetuity.*

  
\_\_\_\_\_  
Author Signature

09/04/2016  
Date